Comparison of Wall Function Model with Low-Reynolds Number Model under Roughness Effect Condition at Actual Ship Scale

Kunihide Ohashi*
*National Maritime Research Institute, Japan
k-ohashi@nmri.go.jp

1 Introduction

The wall function model with a roughness effect is developed and applied to the cases of the two-dimensional(2D) flat plate and flows around the actual ship which has the measured data at the actual sea test. The wall function is composed by a non-dimensionalized roughness height, turbulent kinetic energy and a specific frequency based on the assumption of the local equilibrium. The distributions of the non-dimensionalized velocity based on the non-dimensionalized distance are compared with the curves of the low-Reynolds number model with changing the roughness height and Reynolds number. Additionally, the velocity contours of the wall function method are compared with the results of the low-Reynolds number model and the actual sea test. The applicability of the present method is examined through the detailed comparisons.

2 Computational method

2.1 Base solver

An in-house structured CFD solver (Ohashi et al.(2018)) is employed. The governing equation is 3D RANS equation for incompressible flows. Artificial compressibility approach is used for the velocity-pressure coupling. Spatial discretization is based on a finite-volume method. A cell centered layout is adopted in which flow variables are defined at the centroid of each cell and a control volume is a cell itself. Inviscid fluxes are evaluated by the third-order upwind scheme based on the flux-difference splitting of Roe. The evaluation of viscous fluxes is second-order accurate. The first order Euler implicit scheme is employed for the temporal step. The linear equation system is solved by the symmetric Gauss-Seidel (SGS) method.

The Reynolds stress components are evaluated by one of the linear two equation model, the $k-\omega$ SST model. For free surface treatment, an interface capturing method with a single phase level set approach is employed. The propeller effects are accounted for according to the body forces derived from the propeller model(Ohashi et al.(2018)), which is based on the potential theory.

2.2 Overtset grid method

The weight values for the overset grid interpolation are determined by an in-house system(Kobayashi et al.(2016)). The detail of the system can be found on Kobayashi et al.(2016), the summary is described.

1. The priority of the computational grid is set.
2. The cells of a lower priority grid and inside a body is identified (called as in-wall cell in here).
3. Receptors cells which the flow variables have to be interpolated from donor cells are defined. Two cells on a higher priority grid and facing to the outer boundary are set as receptor cells to satisfy the third order discretization of NS solver. Additionally, two cells neighborhood of in-wall cells, the cells of a lower priority grid and inside the domain of a higher priority grid are also set as the receptor cell.
4. The weight values for the overset interpolation are determined by solving the inverse problem based on Ferguson spline interpolation.

Flow variables of the receptor cell are updated when the boundary condition is set. The forces and moments are integrated on the higher priority grid to eliminate the lapped region on body surfaces. At first, the cell face of the lower priority grid is divided into small pieces. Secondly, the small piece is projected to the cell face of the higher priority grid by using the normal vector of the higher priority

face. Then the 2D solid angle is computed and the small piece is decided in or out of the higher priority face. Once the small piece is in the higher priority face, the area ratio of the piece is set to zero. Finally, the area ratio is integrated on the lower priority face, then we have the ratio to integrate the forces and moments on lower priority face.

2.3 Wall function with roughness model

Non-dimensionalized roughness height is defined by using the frictional velocity u_τ and roughness height h_r as follows:

$$h_r^+ = \frac{u_\tau h_r}{\nu} \tag{1}$$

Non-dimensionalized form of Eq.(2) is given as follows:

$$h_r^+ = u_\tau h_r R \tag{2}$$

Shear stress can be obtained by the following equation applying the wall function.

$$\tau_w = c_\mu^{1/4} k_p^{1/2} \frac{\kappa U_p}{ln\left(\frac{Ey^+}{(1+C_s h_r^+)}\right)} \tag{3}$$

where k_p is the turbulent kinetic energy at the first point away from a wall surface, and the second term is based on the correction formula to take into account the roughness effect suggested by Cebeci(Cebeci et al.(1977)). c_μ is 0.09, E=9.8, $\kappa = 0.41$ and $C_s = 0.3$ based on the assumption of the local equilibrium. U_p is the wall parallel component at the first point away from a wall surface.

The boundary condition of the specific frequency ω on a wall surface is determined by the condition of the dissipation rate ϵ as follows;

$$\epsilon = \frac{C_\mu^{3/4} k_p^{3/2}}{\kappa y_p} \tag{4}$$

$$\omega = \frac{\epsilon}{C_\mu k} \tag{5}$$

where y_p is the distance from the wall surface at the first cell center position.

The velocity profile which is proposed by Apsley(Apsley(2007)) is utilized for the comparison.

$$u^+ = y_{v0}^+ + \frac{1}{\kappa} ln\left(\frac{1+\kappa(y^+ - y_v^+)}{1+\kappa(y_{v0}^+ - y_v^+)}\right) \tag{6}$$

$$y_v^+ = \begin{cases} C - \frac{1}{\kappa} ln(\kappa) & C - \frac{1}{\kappa} ln(\kappa) \geq 0 \\ \frac{1}{\kappa}(1 - e^{-\kappa(C - \frac{1}{\kappa} ln(\kappa))}) & C - \frac{1}{\kappa} ln(\kappa) < 0 \end{cases} \tag{7}$$

$$C = 8 - \frac{1}{\kappa} ln(h_R^+ + 3.152) \tag{8}$$

$$y_{v0}^+ = max(y_v^+, 0) \tag{9}$$

2.4 Uncertainty analysis

Uncertainty analysis based on the Richardson extrapolation method with the FS method(Xing et al.(2010)) is performed. The grid discretization uncertainty is evaluated due the steady condition on the present study, and the three systematic grids with the uniform refinement ratio $r_G = \sqrt{2}$ are utilized. Once, the solutions S_3, S_2, S_1 relevant from the coarse grid to fine grid are obtained, the solution changes are defined as $\epsilon_{12} = S_2 - S_1$, $\epsilon_{23} = S_3 - S_2$. The convergence ratio R is $\epsilon_{12}/\epsilon_{23}$, and R takes the monotonic convergence with $0 < \epsilon_{12}/\epsilon_{23} < 1$. The order of accuracy p and the error δ_{RE} are defined as follows:

$$p = \frac{ln(\epsilon_{23}/\epsilon_{12})}{ln(r_G)}, \quad \delta_{RE} = S_1 - S_0 = \frac{\epsilon_{12}}{r_G^p - 1} \tag{10}$$

The uncertainty is estimated by the following equation using the variable $P = p/p_{th}$. Theoretical accuracy p_{th} is assumed as $p_{th} = 2$.

$$U_{SN} = \begin{cases} (2.45 - 0.85P)|\delta_{RE}|, & 0 < P \leq 1 \\ (16.4P - 14.8)|\delta_{RE}|, & P > 1 \end{cases} \tag{11}$$

3 Computational results

3.1 2D Flat plate case

A 2D flat plate case is selected as the fundamental test case. The Reynolds number is set 1.0×10^7 and 1.0×10^9 based on the plate length L as the reference length. Table 1 shows the computational grids with the three resolutions. Fig. 1 shows the computational grid, the boundary conditions and the definitions of directions of the divisions. The distance between the wall surface and the top boundary is 0.1L.

Table 1: Division number of computational grid

Grid	IM×JM
Coarse(G_3)	193×113
Medium(G_2)	273×161
Fine(G_1)	385×225

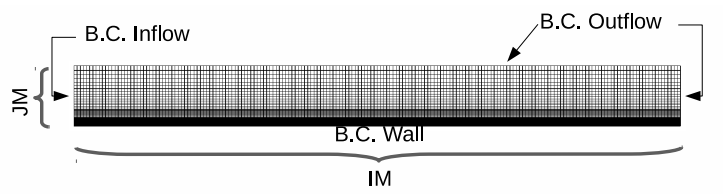

Fig. 1: Computational grid

Table 2 shows the non-dimensionalized distance y^+ and resistance coefficient with changing the minimum spacing on wall at $R = 1.0 \times 10^7$. Although, the resistance coefficient takes higher value at the lower range of y^+, the influence of the minimum spacing on wall is relatively small in the every case with changing the roughness height. The non-dimensionalized distance y^+ is set as 200 hereafter.

Table 2: Resistance coefficient with changing roughness height and minimum spacing on wall ($\times 10^{-3}$, $R = 1.0 \times 10^7$)

y^+	1×10^{-5}	2.5×10^{-5}	5×10^{-5}	7.5×10^{-5}
30	3.034	3.458	3.947	4.323
75	2.985	3.377	3.860	4.216
100	3.061	3.401	3.810	4.134
150	3.026	3.375	3.805	4.147
200	3.061	3.401	3.810	4.134
300	3.128	3.464	3.854	4.155

Table 3 shows the comparison of the resistance coefficient with changing the roughness height from $h_r = 1 \times 10^{-5}$ to $h_r = 7.5 \times 10^{-5}$ and the grid resolutions at the Reynolds number $R = 1.0 \times 10^7$. The roughness height is non-dimensionalized by the plate length L, and the roughness height is selected in the range where the resistance coefficient becomes larger than the value of the smooth surface. Although the uncertainty is resulted in the range from 7% to 17% of the solution of the fine grid, the differences between the three grids are limited within 1%. The results of the wall function indicate from 1% to 3% higher than the result of the low-Reynolds number model(Ohashi(2019)), and the resistance coefficient increases with the roughness height which is similar to the results of the empirical formula.

Table 3: Comparison of resistance coefficient ($\times 10^{-3}$, $R = 1.0 \times 10^7$)

Grid	1×10^{-5}	2.5×10^{-5}	5×10^{-5}	7.5×10^{-5}
Coarse	3.061	3.402	3.810	4.134
Medium	3.072	3.415	3.825	4.152
Fine	3.085	3.429	3.841	4.169
$U_{SN}\%G_1$	7.27	14.52	16.86	16.5
Fine(Low-Re)	3.036	3.295	3.780	4.040
Emp.	2.872	3.350	3.788	4.081

Fig. 2 shows the distribution of u^+ and y^+ with changing the roughness height at the positions $x/L = 0.5$ and $x/L = 0.9$. For the reference, the correlations based on the smooth surface condition and Eq.(6) with the roughness $h_r = 7.5 \times 10^{-6}$ are also shown in Fig. 2. The velocity distributions change at the logarithmic region with the roughness height which is similar to the results of the low-Reynolds number model(Ohashi(2019)), and the first point away from a wall surface locates at $y^+ = 200$ to which is intended.

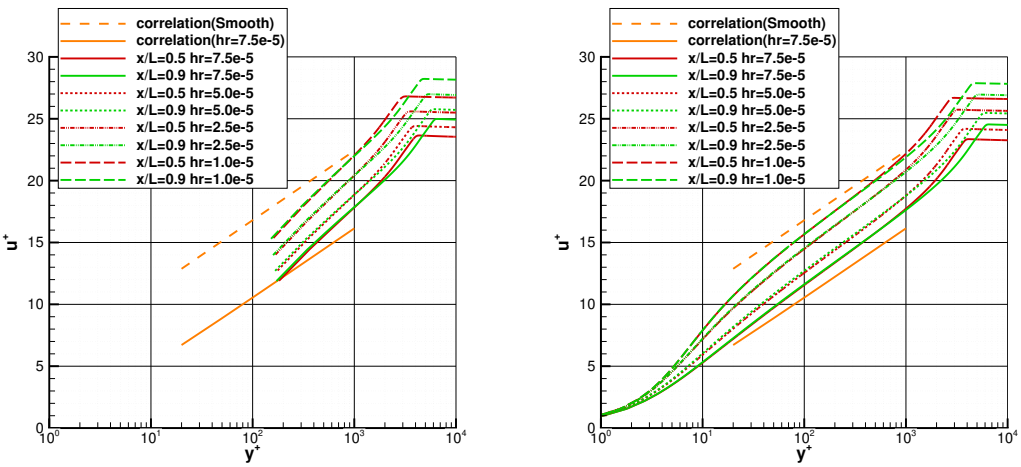

Fig. 2: Comparison of y^+ and u^+ at $R = 1.0 \times 10^7$ (Left: Wall function, Right: Low-Reynolds number model)

Table 4 shows the resistance coefficient with changing the roughness height from $h_r = 1 \times 10^{-7}$ to $h_r = 7.5 \times 10^{-7}$ and the grid resolutions at the Reynolds number $R = 1.0 \times 10^9$. The uncertainty is resulted in the small value which is less than 1%. The difference between the value of the wall function method and the value of the empirical formula is about 2%, and the difference between the value of the wall function method and the value of the low-Reynolds number model results within 5%.

Fig. 3 shows the distribution of u^+ and y^+ with changing the roughness height. The computed results show the similar distribution with the case $R = 1.0 \times 10^7$ excepting the logarithmic region becomes wider

Table 4: Comparison of resistance coefficient ($\times 10^{-3}$, $R = 1.0 \times 10^9$)

Grid	1×10^{-7}	2.5×10^{-7}	5×10^{-7}	7.5×10^{-7}
Coarse	1.513	1.622	1.752	1.853
Medium	1.539	1.652	1.787	1.891
Fine	1.541	1.655	1.790	1.894
$U_{SN}\%G_1$	0.48	0.66	0.52	0.63
Fine(Low-Re)	1.627	1.709	1.845	1.984
Emp.	1.487	1.673	1.837	1.944

than the results of $R = 1.0 \times 10^7$. The first point away from a wall surface with the wall function locates again at $y^+ = 200$, and the distributions take the similar curve with the result of the low-Reynolds number model.

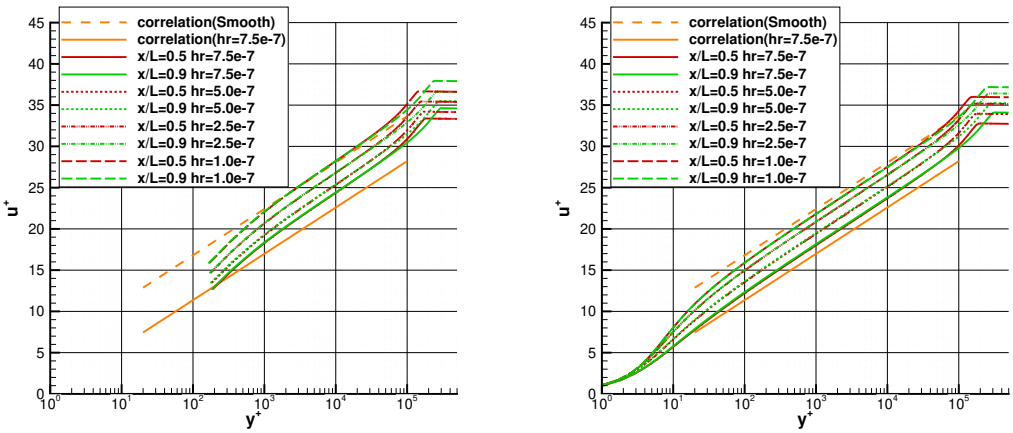

Fig. 3: Comparison of y^+ and u^+ at $R = 1.0 \times 10^9$ (Left: Wall function, Right: Low-Reynolds number model)

Figure 4 shows the distribution of h_r^+ on the flat plate at the condition with $h_r = 7.5 \times 10^{-7}$. h_r^+ takes larger value near the front end of the flat plate, then, the value becomes almost constant value with $h_r^+ = 25$ over the surface.

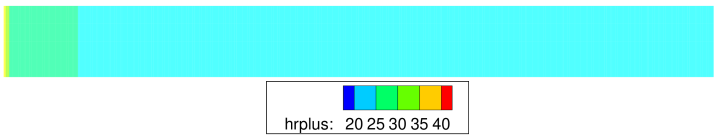

Fig. 4: Non-dimensionalized roughness height on the wall($h_r = 7.5 \times 10^{-7}$, $R = 1.0 \times 10^9$)

3.2 Actual ship scale

The wall function with the roughness effect is applied to the case with the tanker hull(CFD W.S.(1994)) which has the flow measurement data of the actual ship. The computations are carried out on the propulsive condition with the free surface effect. The Reynolds number based on the ship length L is $R = 2.43 \times 10^9$, and the Froude number is $Fn = 0.153$. Propulsive condition is achieved by using the propeller model, and propeller rotational speed and thrust are adjusted to be equal to the resistance of the ship. The roughness value is set $150 \times 10^{-6} m$ based on the ITTC recommended procedure(ITTC R.P. 7.5-02-03-01.4,).

Table 5 shows the division number of computational grids in each direction. The grids are arranged with the priority of the overset interpolation. The computational grid is consisted from the hull grid, the

rudder grid and two rectangular grids including the refinement grid near the aft part of the ship hull and the grid covering the whole domain.

Fig. 5 shows the global view of the computational grids with the boundary conditions and the grids near the aft part of the hull. The minimum spacing on the wall surface is set to $y^+ = 200$.

Table 5: Division number of computational grid

Grid	Coarse IM×JM×KM	Medium IM×JM×KM	Fine IM×JM×KM
Rudder	45×69×35	61×97×49	85×137×69
Refined Rect.	45×33×45	45×33×45	45×33×45
Hull	141×145×41	197×209×57	277×305×81
Rect.	337×89×57	337×89×57	337×89×57

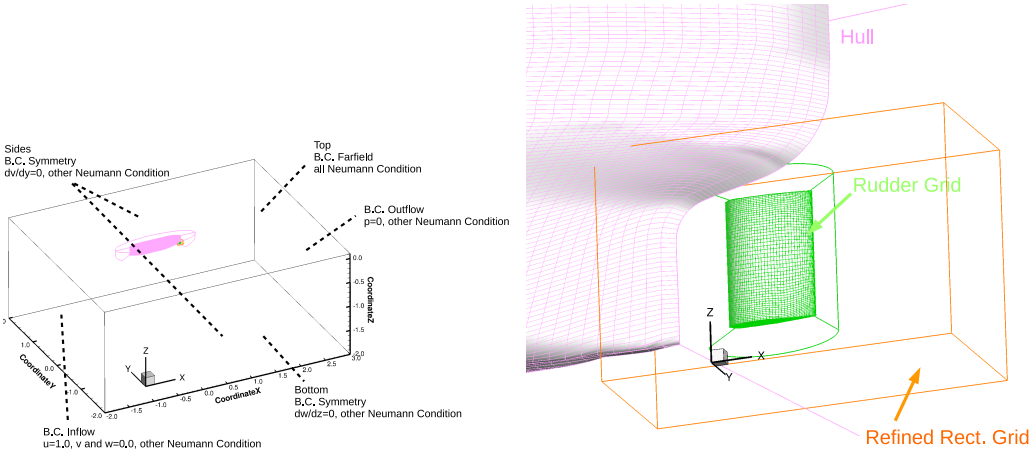

Fig. 5: Computational grid (Left:global view, Right:near aft part of hull)

Fig. 6 shows the comparisons with the measured data of the actual ship. The position is x/L=0.98533 from the fore perpendicular position. The results with the roughness effect show agreement with the measured data, especially, the range $u/U = 0.5 - 0.7$. The differences between the result of the grid resolutions are slightly small. Fig. 7 shows the comparison between the results with the wall function and the data with the low-Reynolds number model(Ohashi(2019)). The difference between the results of the wall function and the low-Reynolds number model is slightly small, and the both results with the roughness effect show good agreement with the measured data of the actual ship.

Finally, figure 8 shows the distribution of the non-dimensionalized roughness height h_r^+ on the body surfaces. h_r^+ takes small value near the fore and stern end, and h_r^+ is distributed on the body surface with the value near 40. The difference between the port and starboard sides is slightly small. The non-dimensionalized roughness height on the rudder surface which is positioned behind the propeller takes higher value than h_r^+ on the hull surface. The difference between the port and starboard sides on the rudder surface can be observed which is affected by the propeller rotational flow. h_r^+ with the wall function show similar distribution of the low-Reynolds number model on the hull surface except the region near the fore and stern ends, and h_r^+ distributions on the rudder surface take similar shapes, and the values of h_r^+ of the wall function are resulted in larger value than the results of the low-Reynolds number model.

4 Conclusion

The wall function including the roughness effect is developed and applied to the cases at the high Reynolds number on the actual ship scale. At first, the present method is applied to the 2D flat plate case with changing the roughness height and Reynolds number. The resistance coefficients of the wall

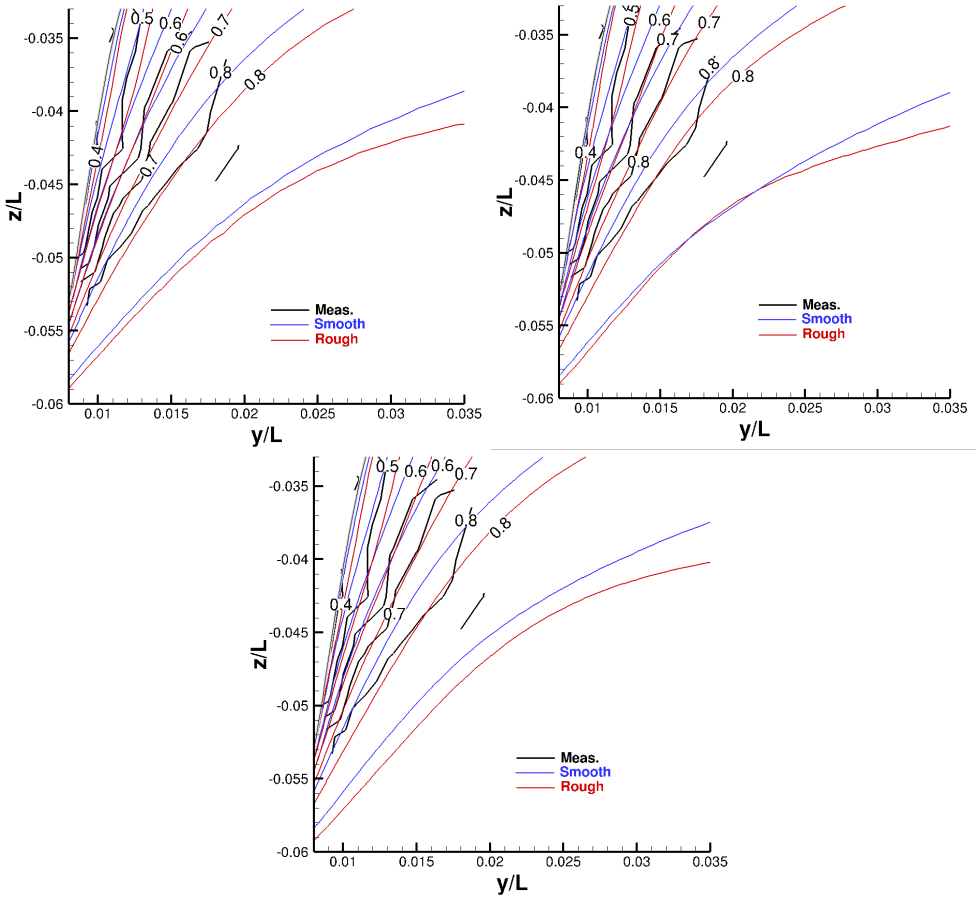

Fig. 6: Axial velocity contour(Top left:Coarse grid, Top right:Medium grid, Bottom:Fine grid)

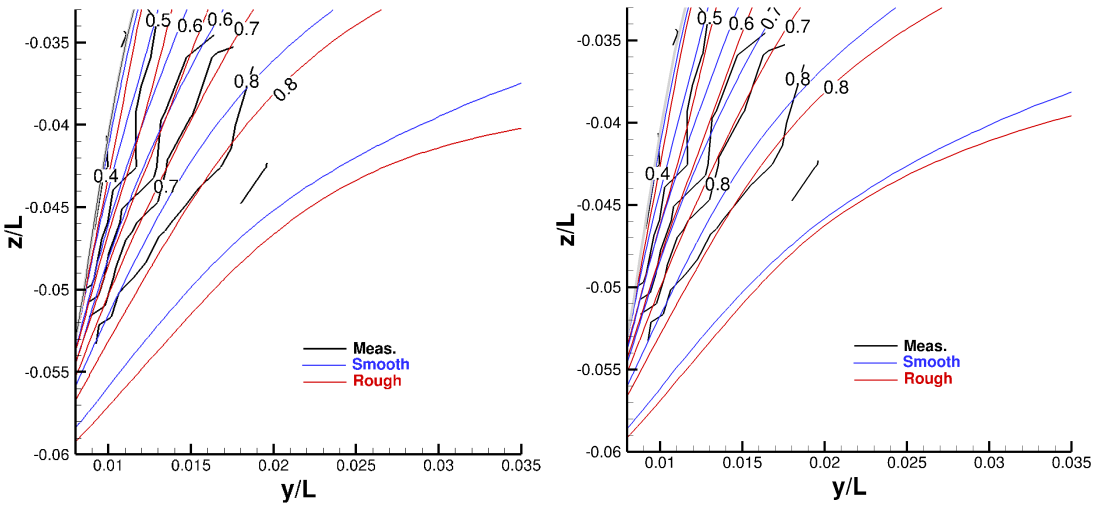

Fig. 7: Axial velocity contour(Left: Wall function, Right: Low-Reynolds number model)

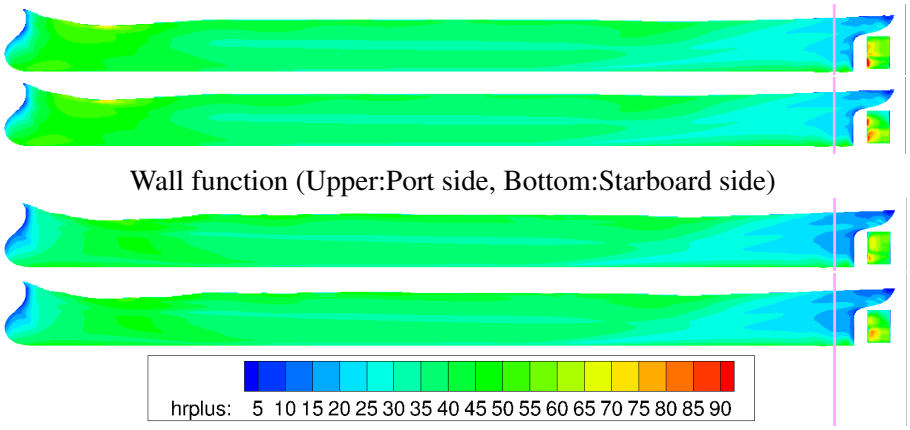

Wall function (Upper:Port side, Bottom:Starboard side)

Low-Reynolds number model (Upper:Port side, Bottom:Starboard side)

Fig. 8: Non-dimensional roughness on the hull and rudder surfaces

function close to the values of the low-Reynolds number model and the empirical formula, and the distributions of the non-dimensional velocity u^+ based on y^+ decrease with the increase of the roughness height and show the similar curves of the low-Reynolds number model. Next, the present wall function method is applied to the flows around the tanker ship, and the velocity distributions with the roughness effect show agreement with the measured data of the actual ship as similar with the results with the low-Reynolds number model.

References

K. Ohashi et al. (2018). Development of a structured overset Navier-Stokes solver including a moving grid with a full multigrid method, JMST.

H. Kobayashi and Y. Kodama. (2016). Developing Spline Based Overset Grid Assembling Approach and Application to Unsteady Flow Around a Moving Body, Journal of Mathematics and System Science 6, pp.339-347.

T. Cebeci and P. Bradshow. (1977). Momentum Transfer in Boundary Layers, Hemisphere Publishing Corporation, Series in Thermal and Fluids Engineering.

D.C. Wilcox. (2006). Turbulence modeling for CFD, Third Edition, DCW Industries.

L. Eça, M. Hoekstra. (2011). Numerical aspects of including wall roughness effects in the SST $k-\omega$ eddy-viscosity turbulence model, Comp. and Fluids, Vol.40, pp.299-314.

A. Hellsten. (1997). Some improvements in Menter's $k-\omega$ SST AIAA-98-2554.

D. Apsley. (2007). CFD calculation turbulent flow with arbitrary wall roughness, Flow Turb. Comb., Vol.78, pp.153-175.

T. Xing, , F. Stern. (2010). Factors of safety for Richardson extrapolation, J. Fluids Eng., Vol.132(6).

A. Mills, X. Hang. (1983). On the skin friction coefficient for a fully rough flat plate, Trans. ASME, J. Fluids Eng., Vol.105, pp.364-365.

K. Ohashi. (2019). Numerical Study of Roughness Model Effect at Actual Ship Scale, ECCOMAS MARINE 2019.

Proc. of CFD Workshop Tokyo 1994.

ITTC recommended procedures and Guidelines 7.5-02-03-01.4, 1978 ITTC Performance Prediction Method.